

# Radiation dose reduction in computed tomography perfusion using spatial-temporal Bayesian methods

Ruogu Fang<sup>\*a</sup>, Ashish Raj<sup>b</sup>, Tsuhan Chen<sup>a</sup>, Pina C. Sanelli<sup>b</sup>

<sup>a</sup>Dept. of Electrical and Computer Engineering, Cornell University, Ithaca, NY, USA 14853;

<sup>b</sup>Dept. of Radiology, Weill Cornell Medical College, New York, NY USA 10065

## ABSTRACT

In current computed tomography (CT) examinations, the associated X-ray radiation dose is of significant concern to patients and operators, especially CT perfusion (CTP) imaging that has higher radiation dose due to its cine scanning technique. A simple and cost-effective means to perform the examinations is to lower the milliampere-seconds (mAs) parameter as low as reasonably achievable in data acquisition. However, lowering the mAs parameter will unavoidably increase data noise and degrade CT perfusion maps greatly if no adequate noise control is applied during image reconstruction. To capture the essential dynamics of CT perfusion, a simple spatial-temporal Bayesian method that uses a piecewise parametric model of the residual function is used, and then the model parameters are estimated from a Bayesian formulation of prior smoothness constraints on perfusion parameters. From the fitted residual function, reliable CTP parameter maps are obtained from low dose CT data. The merit of this scheme exists in the combination of analytical piecewise residual function with Bayesian framework using a simpler prior spatial constrain for CT perfusion application. On a dataset of 22 patients, this dynamic spatial-temporal Bayesian model yielded an increase in signal-to-noise-ratio (SNR) of 78% and a decrease in mean-square-error (MSE) of 40% at low dose radiation of 43mAs.

**Keywords:** spatial-temporal, Bayesian, piece-wise, CT perfusion, dose reduction

## 1. INTRODUCTION

Radiation exposure from computed tomography (CT) has raised considerable public concern regarding its potential adverse effects on patients, especially for cancer induction and birth defects. Specifically, CT perfusion (CTP) is a functional imaging study that has higher radiation dose due to its cine scanning technique resulting in numerous images performed repetitively on a focused region of the body. In brain CTP, the cine scanning technique captures the first pass of contrast through the brain to assess its hemodynamic properties at the capillary level, including the cerebral blood flow (CBF), cerebral blood volume (CBV) and mean transit time (MTT).

The tube current used in CTP protocols may range from 150 - 200 mA. High radiation doses used in CTP have been reported to cause biological effects, particularly hair loss<sup>1</sup>. Other disadvantages of CTP include its narrow scanning range and contrast reactions<sup>2,3</sup>. However, CTP is still clinically indispensable compared to other perfusion techniques such as magnetic resonance perfusion (MRP)<sup>4,5</sup> due to its widespread availability, rapid acquisition time and superior spatial resolution. In addition, CTP provides absolute quantitative data based on the relationship between the CT value, known as the Hounsfield unit, and the iodine concentration. Sasaki et al.<sup>6</sup> provide a comprehensive overview on the advantages of CTP, which has been widely applied in evaluating perfusion abnormalities of acute stroke patients<sup>7,8,9</sup>.

Therefore, recent efforts have been focused on promoting safe and appropriate utilization of CT scanning techniques to reduce the radiation exposure while maintaining the quality of images. However, reduction of tube current and therefore radiation dose results in image artifacts and noise. This quality degradation becomes more obvious in perfusion maps that already have low SNR because it measures the dynamic change of the contrast concentration in the blood. Hence inordinate dose reduction could potentially lead to inaccurate diagnosis and even erroneous clinical decisions.

---

\* rf294@cornell.edu; chenlab.ece.cornell.edu

This publication was made possible by Grant Number 5K23NS058387-02 from the National Institute of Neurological Disorders and Stroke (NINDS), a component of the National Institutes of Health (NIH). Its contents are solely the responsibility of the authors and do not necessarily represent the official view of NINDS or NIH.

In this paper, we tackle the problem of restoring noisy CTP parameters resulting from ultra-low radiation dose by proposing a simple explicit piecewise model to capture the essential dynamics of CT perfusion. Then we estimate the model parameters in a Bayesian framework using prior spatial smoothness constraints. Finally we relate model parameters to conventional CTP measures. Our proposal is unique in both the dynamic model and in the form of the constraints to be minimized.

## 2. APPROACH

### 2.1 Conventional Approach to Perfusion Parameter Estimation

Meier and Zieler<sup>10</sup> proved that the time concentration curve (TCC) is the product of CBF and the artery input function (AIF) convolved with the impulse residual function (IRF)  $R$ :

$$C_{tissue}(t) = CBF \cdot AIF(t) \otimes R(t) = CBF \cdot \int_0^t AIF(\tau) \cdot R(t - \tau) d\tau \quad (1)$$

where  $\otimes$  is the convolution operator, and  $t$  is the time step. In this equation,  $C_{tissue}$  and AIF are measured directly from TCC.

Methods to compute CBF and MTT from  $C_{tissue}$  and AIF include the non-deconvolution based max slope method<sup>11</sup>, deconvolution based Fourier transform (FT) approach<sup>12,13,14</sup>, singular value decomposition (SVD)<sup>15,16</sup> and block circulant SVD<sup>17</sup>. In our work, we used block circulant SVD which corrects for delay and dispersion of the AIF with a trace-arrival time-insensitive technique. CBF and MTT maps were computed by deconvolving the block circulant AIF matrix. CBV was calculated by multiplying CBF and MTT based on the central volume theory<sup>10</sup>. Although the deconvolution approach is widely used, it suffers from noise amplification and ill-conditioning present in the inversion of any linear system.

### 2.2 A New Dynamic Model-Based Approach

In order to recover useful information from noisy and inadequate raw data, it is usually necessary to impose additional constraints on the solution being sought. We now propose an approach that relies on both a simple model for the residual function as well as additional spatial-temporal constraints on the parameters to be determined.

We model the unit impulse residual function  $R(t)$  by an analytical piecewise function

$$R_{\tau,t_0}(t) = \begin{cases} 0 & t < t_0 \\ e^{-\frac{t-t_0}{\tau}} & t \geq t_0 \end{cases} \quad (2)$$

given perfusion parameters  $\tau$  and the delay time  $t_0$ . This exponential model for the impulse residue function has been proposed by Østergaard et. al.<sup>12</sup> and has been successfully used for modeling the delaying contrast in the vessels. Using the convolution formula (1) we relate the observed data to the model via an additive noise term  $n(\mathbf{r}, t)$ .

$$C_{tissue}(\mathbf{r}, t) = CBF(\mathbf{r}) \cdot AIF(t) \otimes R_{\tau,t_0}(\mathbf{r}, t) + n(\mathbf{r}, t) \quad (3)$$

where  $\mathbf{r} = (x, y, z)$  is the position of the tissue.

### 2.3 Energy Function

Following previous work in Bayesian image denoising<sup>18,19</sup>, we model the additive noise with a white Gaussian  $n(\mathbf{r}, t) \sim \mathcal{N}(0, \sigma_n^2)$ , and propose the likelihood function

$$\Pr(C_{tissue}(\mathbf{r}, t) | \tau, t_0, CBF) \sim \exp\left(-\frac{1}{T} \frac{\sum_t (C_{tissue}(\mathbf{r}, t) - CBF(\mathbf{r}) \cdot AIF(t) \otimes R_{\tau,t_0}(\mathbf{r}, t))^2}{2 \sigma_n^2}\right) \quad (4)$$

This basically encodes the expectation that after the residual model at any location in the image has convolved with AIF, the resulting signal should be different from the observation only by the amount of additive noise present in the instrumentation. A direct maximization of the above likelihood will result in a conventional least squares minimization problem, which is easily solvable by a linear pseudo-inverse operation<sup>20</sup>.

However, due to the highly noisy scenarios in low dose CTP, it is necessary to impose additional constraints in the form of prior knowledge about the parametric images we wish to obtain. Specifically, we wish the solution to have both temporal and spatial coherence observed in real brain data, whereby the perfusion parameters ( $\tau$ ,  $t_0$ , etc) change smoothly across the image as well as across the temporal acquisition window. However, we must apply these constraints adaptively in order to avoid indiscriminate smoothing across tissue boundaries.

Here we propose a simpler model that nevertheless is highly effective for CTP data. Since the voxel dimensions in a typical CTP image are much smaller than tissue structures of interest, it is reasonable to assume that within extended neighborhoods the perfusion parameters will be constant. In reality, perfusion parameters are spatially variable due to the combined effect of scanner blurring, reconstruction algorithm, physiological noise and natural tissue variability. While most of these sources of variability are local, scanner blurring is best captured in terms of a convolution kernel across several neighboring voxels.

Unfortunately, these kinds of priors will lead to extended neighborhood interactions which might necessitate MRF approaches – something we wish to avoid. Therefore we propose a much simpler prior formulation, which is nonetheless physically and clinically realistic. The perfusion parameter  $\tau$  at any location  $\mathbf{r}$ , at the center of a spatially homogeneous neighborhood  $\mathcal{N}_r$ , is given by the Gaussian distribution

$$\Pr(\tau(\mathbf{r})) \sim \exp\left(-\frac{(\tau(\mathbf{r}) - \mu_\tau(\mathcal{N}_r))^2}{2 \sigma_\tau^2(\mathcal{N}_r)}\right) \quad (5)$$

where  $\mu_\tau$  and  $\sigma_\tau$  are the mean and standard deviation of  $\tau$  within the neighborhood  $\mathcal{N}_r$ . Similarly we define

$$\Pr(t_0(\mathbf{r})) \sim \exp\left(-\frac{(t_0(\mathbf{r}) - \mu_{t_0}(\mathcal{N}_r))^2}{2 \sigma_{t_0}^2(\mathcal{N}_r)}\right) \quad (6)$$

$$\Pr(\text{CBF}(\mathbf{r})) \sim \exp\left(-\frac{(\text{CBF}(\mathbf{r}) - \mu_{\text{CBF}}(\mathcal{N}_r))^2}{2 \sigma_{\text{CBF}}^2(\mathcal{N}_r)}\right) \quad (7)$$

By allowing the local mean and variance to change across the image, the simple Gaussian model is able to capture the essential variability of the data, but in the process it introduces additional quantities which must be estimated from the true distribution of  $\tau$ , which in turn is unknown a priori. This necessitates an Expectation Maximization (EM)<sup>21</sup> style approach whereby the Gaussian parameters and the underlying quantity are estimated alternately. It is well known that EM algorithms have guaranteed convergence starting from arbitrary initial estimates. Given a sufficiently large local neighborhood  $\mathcal{N}_r$ , we expect that the local Gaussian parameters can be estimated accurately.

Bayesian estimation using Eqs (4-7) is a well known problem, and involves maximizing the posterior distribution

$$\Pr(\tau, t_0, \text{CBF} | C_{\text{tissue}}(\mathbf{r}, t)) \propto \Pr(C_{\text{tissue}}(\mathbf{r}, t) | \tau, t_0, \text{CBF}) \Pr(\tau(\mathbf{r})) \Pr(t_0(\mathbf{r})) \Pr(\text{CBF}(\mathbf{r})) \quad (8)$$

Here we have assumed that the parametric processes  $\tau, t_0, \text{CBF}$  are independent of each other for computational tractability. This is easily converted to an equivalent minimization problem

$$\langle \hat{\tau}(\mathbf{r}), \hat{t}_0(\mathbf{r}), \hat{\text{CBF}}(\mathbf{r}) \rangle = \arg \min_{\tau, t_0, \text{CBF}} \left\{ \begin{array}{l} \frac{1}{T} \frac{\sum_t (C_{\text{tissue}}(\mathbf{r}, t) - \text{CBF}(\mathbf{r}) \cdot \text{AIF}(t) \otimes R_{\tau, t_0}(\mathbf{r}, t))^2}{2 \sigma_n^2} \\ + \frac{(\tau(\mathbf{r}) - \mu_\tau(\mathcal{N}_r))^2}{2 \sigma_\tau^2(\mathcal{N}_r)} + \frac{(t_0(\mathbf{r}) - \mu_{t_0}(\mathcal{N}_r))^2}{2 \sigma_{t_0}^2(\mathcal{N}_r)} + \frac{(\text{CBF}(\mathbf{r}) - \mu_{\text{CBF}}(\mathcal{N}_r))^2}{2 \sigma_{\text{CBF}}^2(\mathcal{N}_r)} \end{array} \right\} \quad (9)$$

Unfortunately, the joint minimization of even this simplified model is challenging due to the large number of variables, non-convexity, and unknown local Gaussian parameters. We will now make several simplifying observations and propose a realistic algorithm for (approximately) solving Eq. 9.

## 2.4 A Fast EM-style Algorithm for Spatial-Temporal Bayesian Method

We first note that a robust estimate of the delay  $t_0$  is in fact easy to calculate from the tissue concentration peak location (Fig 1), and its value should not change significantly due to other unknowns. Of course, additive noise can cause spurious peaks; however, this is easily corrected by a simple temporal smoothing operation on  $C_{\text{tissue}}(\mathbf{r}, t)$  before peak detection. Therefore our first simplification is to estimate  $t_0$  directly from observed data (after upsampling and smoothing operations) and henceforth remove it from the equation.

Another simplification results from the observation that  $\text{CBF}(\mathbf{r})$  is simply the ‘‘height’’ of the residual function, and is roughly given by dividing the peak value of the observed tissue concentration curve by the peak value of  $\text{AIF}(t) \otimes R_{\tau, t_0}(\mathbf{r}, t)$  at each voxel. Finally, we noted that estimates of variance from current estimates of perfusion parameters is usually under-estimated by sample standard deviation, necessitating a minor correction for unusually small variances. Putting these points together, we propose the following algorithm

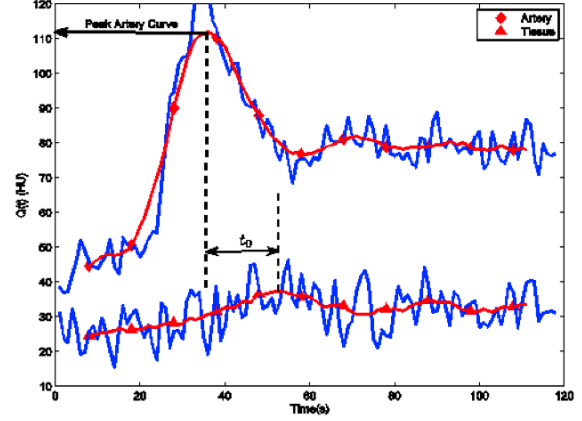


Fig. 1. Delay between Artery Input Function (AIF) and tissue concentration curve(TCC)

---

### Algorithm: Fast EM-style Algorithm for Spatial-Temporal Bayesian Method

---

- Start iteration  $i = 0$  with  $\tau_0, t_0$  and  $\text{CBF}_0$  estimated by conventional deconvolution technique
  - Then for  $i = 1, \dots, n_{\text{iters}}$ 
    1.  $\widehat{\text{CBF}}_i(\mathbf{r}) = \max_t \frac{C_{\text{tissue}}(\mathbf{r}, t)}{\text{AIF}(t) \otimes R_{\tau_{i-1}, t_0}(\mathbf{r}, t)}$
    2. Draw a circular neighborhood  $\mathcal{N}_r$  of radius  $R$  around each point  $\mathbf{r}$  and estimate local Gaussian parameters  $\mu_\tau, \mu_{\text{CBF}}, \sigma_\tau, \sigma_{\text{CBF}}$  from samples of  $\tau_{i-1}, \text{CBF}_{i-1}$  in each neighborhood
    3.  $\text{CBF}_i(\mathbf{r}) = \arg \min_{\text{CBF}} \left\{ \left( \widehat{\text{CBF}}_i(\mathbf{r}) - \text{CBF}(\mathbf{r}) \right)^2 + \gamma^2 \frac{(\text{CBF}(\mathbf{r}) - \mu_{\text{CBF}}(\mathcal{N}_r))^2}{\sigma_{\text{CBF}}^2(\mathcal{N}_r) + \Delta t} \right\}$
    4.  $\tau_i(\mathbf{r}) = \arg \min_{\tau} \left\{ \frac{1}{T} \sum_t (C_{\text{tissue}}(\mathbf{r}, t) - \text{CBF}_i(\mathbf{r}) \cdot \text{AIF}(t) \otimes R_{\tau, t_0}(\mathbf{r}, t))^2 + \beta^2 \frac{(\tau(\mathbf{r}) - \mu_\tau(\mathcal{N}_r))^2}{\sigma_\tau^2(\mathcal{N}_r) + \Delta t} \right\}$   
under the constraint
$$\tau_{\min} \leq \tau_i(\mathbf{r}) \leq \tau_{\max}$$
  - Repeat until convergence
- 

Table 1. Algorithm of fast EM-style spatial-temporal Bayesian method

Note here we add a small constant  $\Delta t$  to avoid very large terms in case of very small estimates of standard deviation of the local Gaussians. Here we set  $\Delta t$  to be 1. Since the noise variance  $\sigma_n$  is essentially unknown in realistic situations we subsume it within the new global ‘‘regularization’’ parameters  $\gamma$  and  $\beta$ . The Gaussian fits over an extended local neighborhood allows for the imposition of spatial coherence without resorting to MRF approaches that are computationally prohibitive. The radius  $R$  of the neighborhood, as well as spatial coherence weight  $\beta$  are important algorithmic parameters whose optimal value is not known a priori. A larger  $R$  and larger  $\beta$  will both cause smoother perfusion maps. Once best parameters of the model in Eq. 9 are known, the clinically relevant perfusion parameters are directly calculated:

$$\text{MTT}(r) = \int_0^{\infty} R(r, t) dt = \int_0^{t_0} dt + \int_{t_0}^{\infty} e^{-\frac{t-t_0}{\tau}} dt = t_0 + \tau \quad (10)$$

$$\text{CBV}(r) = \text{CBF}(r) \cdot \text{MTT}(r) \quad (11)$$

where the last relation comes from the central volume theory<sup>17, 22</sup>.

### 3. EXPERIMENTAL DETAILS

#### 3.1 CTP Scanning Protocol and Data Processing

CTP was performed on aneurysmal subarachnoid hemorrhage patients under an existing IRB-approved clinical trial with our standard scanning protocol for CTP at our institution using GE Lightspeed or Pro-16 scanners (General Electric Medical Systems, Milwaukee, WI) with cine 4i scanning mode and 45 second acquisition at 1 rotation per second using 80 kVp and 190 mA.

Post-processing of the acquired images into CBF, CBV and MTT maps were performed on a GE Advantage Workstation using CTP software version 3.0 (General Electric Medical Systems). This software employs a deconvolution method involving the block circulant SVD approach, which is considered most accurate for low contrast injection rates<sup>23</sup>. Both data at the standard radiation dose of 190mA and from the simulated low dose of 10mA were processed.

#### 3.2 Noise Simulation

Repetitive scanning at different tube current levels on the same patient was not appropriate given the ethical issues raised with the cumulative amount of radiation exposure that would occur. Therefore we simulated images at lower tube current levels by adding statistical noise in a manner similar to methods described by Britten et al.<sup>24</sup>. This model was based on the inverse relationship between the tube current ( $I$ ) and the noise standard deviation ( $\sigma$ ) in CT images

$$\sigma = \frac{K}{\sqrt{I}} \quad (12)$$

We compute the value of  $K$  by analyzing the Gaussian noise in the CTP images of 22 patients under  $I_0 = 190\text{mA}$  dosage, and find the average  $K$  value of  $103.09 \text{ mA}^{1/2}$ . The standard deviation of Gaussian noise ( $\sigma$ ) at low mA exposure setting ( $I$ ) is simulated by adding statistical noise to the CT images scanned at  $I_0$  mA with noise standard deviation of  $\sigma_0$  using the modified equation

$$\frac{\sigma}{\sigma_0} = \frac{\sqrt{I_0}}{\sqrt{I}} \quad (13)$$

The noise distribution is statistically independent, so the standard deviation of the noise distribution to be added ( $\sigma_a$ ) can be computed from

$$\sigma^2 = \sigma_0^2 + \sigma_a^2 \quad (14)$$

We add statistical noise with standard deviation  $\sigma_a = 13.7$  at  $I_0 = 190$  mA and the corresponding radiation exposure is

$$I = \frac{I_0 \cdot \sigma_0^2}{\sigma^2} = \frac{I_0 \cdot \sigma_0^2}{\sigma_0^2 + \sigma_a^2} = \frac{K^2}{\frac{K^2}{I_0} + \sigma_a^2} = \frac{K^2 \cdot I_0}{K^2 + \sigma_a^2 \cdot I_0} = 43.6 \text{ mA} \quad (15)$$

#### 3.3 Implementation of EM-Style Algorithm

We implemented the EM-style using MATLAB 2010b. For the energy minimization in Step 3 of our proposed EM-style algorithm, we use trust-region-reflective algorithm to handle the bound constraints of the perfusion parameters. This algorithm is a subspace trust-region method and it is based on the interior-reflective Newton method. Each iteration involves the approximate solution of a large linear system using the method of preconditioned conjugate gradients (PCG). The maximum number of iterations for the trust-region-reflective is 40, however it usually takes only around 10 iterations to reach the desired minimum value, i.e. change in the residual was less than the specified tolerance. The

termination tolerance we use for the function value is  $10^{-6}$ , and the termination tolerance for  $x$  is also  $10^{-6}$ . The number of PCG iterations is zero for most voxels in the data. We do not provide user-defined Jacobian information and the algorithm approximates the Jacobian using finite difference. On a Windows desktop with Intel Core 3G Hz Duo CPU and 3GB RAM, the program takes 20 minutes to run for the entire  $512 \times 512 \times 118$  3D volumetric brain CTP data of one patient.

The upper bound of MTT and CBF were empirically determined from the CTP data performed at a standard dose. The normal range of MTT is between 0 to 5 seconds, and can be up to 20 seconds at specific areas of the brain, especially in disease states. The range of CBF is between 0 and 80 mL/100g/min, and can be up to 100-150 mL/100g/min in specific areas of hyper-vascular flow.

### 3.4 Parameter Tuning

The three parameters  $\beta$ ,  $\gamma$  and neighborhood radius  $r$  are tuned by a full-search on a validation set of five patients' data. We use two metrics to evaluate the quality of the perfusion maps in the parameter search: Mean Square Error (MSE) and Peak Signal-to-Noise Ratio (PSNR). The optimal parameters found are  $\beta = 10^3$ ,  $\gamma = 10$ , and  $r = 3$ . We assume the parameters are applicable to other patients' data, because the underlying noise model is the same for all low-dose CTP.

## 4. EXPERIMENTAL RESULTS

### 4.1 Evaluation Metrics

Our proposed spatial-temporal Bayesian method is validated on CTP images of 22 patients stored on the Research Picture Archiving and Communications System (PACS) at our institution. Three visual quality assessments are used to examine the restored MTT maps: mean square error (MSE), noise quality measure (NQM) and signal-to-noise ratio (SNR). These three metrics reflect different aspects of the visual quality of static images with additive noise. In combination, they provide a complementary quantitative evaluation of the perfusion maps. MSE represents the difference between optimized MTT maps and the 190mA reference MTT maps. SNR reflects the ratio of signal power to the noise power that corrupts the signal. NQM depicts the image quality by computing the nonlinear weighted signal-to-noise ratio of the restored image with respect to the reference image.

### 4.2 Baselines

Three image denoising techniques to restore static images with additive noise are compared with our proposed Spatial-temporal Bayesian (STB) method. These denoising methods include Gaussian smoothing filter, median filter and anisotropic diffusion (AD)<sup>25,26</sup>. The parameters for each method are tuned on a training set of 5 patients' data, and remain constant for all the experiments. The window size for Gaussian filter is  $6 \times 6$ . The window size for the median filter is  $7 \times 7$ . Anisotropic diffusion is performed with a maximum of 15 iterations, an integration constant of  $1/7$ , and a gradient modulus threshold of 30.

### 4.3 Quantitative Results

Table 2 shows the average quantitative visual assessments on 22 patients. STB is compared with the three baseline methods using the aforementioned assessment metrics, with relative changes from the pre-processed maps reported. A one-tail statistical t-test is performed to analyze the difference between the improvements using our proposed method and the other three denoising methods. STB outperforms the three existing denoising methods on all three visual quality assessment metrics, in spite of the variations in different patients. The overall average performance and the individual cases of 22 patients all demonstrate the advantages of STB. This is because both the temporal consistency and the spatial coherence information are used for noise removal. T-test also reveals that STB is significantly better than the other three methods.

On further analysis, we reveal the relative changes with regard to the unenhanced low dose MTT maps in the brackets. STB reduces MSE by 39% on average, while the Gaussian filter, the median filter, and the anisotropic diffusion reduce MSE by 14%, 26% and 19% respectively. There is an even greater difference seen in the SNR. STB achieves an increase of 78.50%, while the Gaussian filter improves by only 25.60%, the median filter by 53.24% and the anisotropic diffusion by 24.47%. In terms of NQM, STB also performs better than the three other denoising methods that only consider

Metrics	Pre	STB	Change	Gaussian	Change	Median	Change	Diffusion	Change
MSE (sec <sup>2</sup> )	27.40	<b>16.57</b>	-39.53%	23.50	-14.23%	20.16	-26.42%	22.20	-19.00%
NQM (dB)	25.37	<b>27.73</b>	9.30%	26.05	2.68%	27.32	7.69%	27.09	6.78%
SNR (dB)	2.93	<b>5.23</b>	78.50%	3.68	25.60%	4.49	53.24%	3.94	24.47%

Table 2. Quantitative evaluations comparing STB to three baseline methods

spatial coherence. STB improves NQM by 9.3% while the Gaussian filter increases by 2.68%, the median filter by 7.69% and the anisotropic diffusion by 6.78%.

#### 4.4 Qualitative Evaluations

Figure 2 displays the qualitative comparison of the pre- and the post- processing MTT maps using our proposed method and the other three baseline methods in comparison with the standard 190mA maps. The enhanced spatial coherence and resolution using our proposed method (STB) largely improve the quality of the MTT map, and enhance the clinical applicability of CTP at lower radiation dose. In spite of the variations in patients, anatomical structures and cerebral hemodynamic patterns, both quantitative and qualitative comparisons demonstrate the improvement in the spatial and contrast resolution and the decrement in image noise and artifacts that can potentially enhance the clinical value of perfusion images for diagnosis of diseases such as acute stroke.

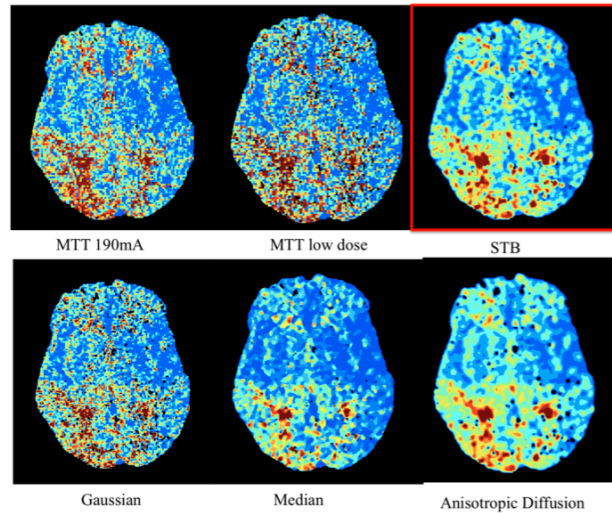


Fig. 2. Analysis of low radiation dose MTT map before and after optimization using our algorithm, Gaussian filter, median filter and anisotropic diffusion, compared to the 190mA standard map. (Best viewed in color)

#### 4.5 Evaluation on Regions of Interest

We also analyzed the denoising effect on different ROIs of the brain in order to understand the effectiveness of our denoising algorithm on various anatomical brain tissues, including white matter, gray matter (cortex), and deep gray matter. The qualitative and quantitative comparison of noisy and optimized low dose CBF, CBV and MTT maps compared with standard 190mA maps are shown in Figure 3 and Table 3. The post-processed perfusion maps on ROIs capture the salient information of CBF, CBV and MTT maps, improve the spatial and contrast resolution, while removing the noise caused by the low radiation dose.

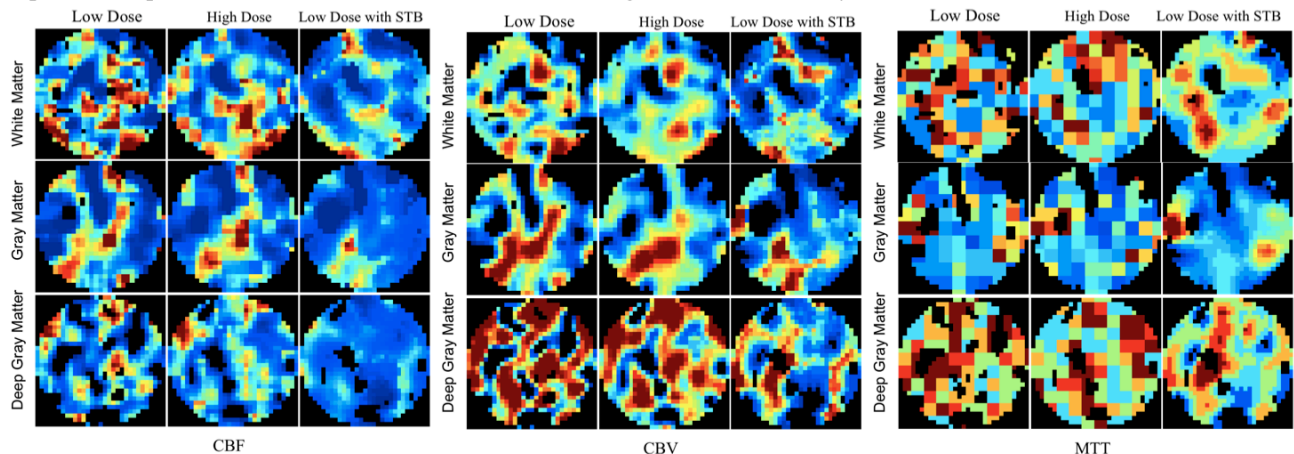


Fig. 3. Comparisons of low dose, high dose and optimized low dose CBF, CBV and MTT maps on regions of interest: White Matter, Gray Matter, and Deep Gray Matter (cortex). (Best viewed in color)

Tissue	CBF (ml/100g/min)			CBV (ml/100g)			MTT (sec)		
	Pre	Post	Change	Pre	Post	Change	Pre	Post	Change
WM	420	<b>298</b>	-29%	26	0.76	-97%	14	5	-65%
GM	307	<b>213</b>	-31%	6	0.76	-87%	29	13	-56%
DGM	393	<b>280</b>	-29%	19	1.01	-94%	14	8	-44%

Table 3. Mean-square-error on regions of interest for CBF, CBV and MTT maps before and after denoising

## 5. LIMITATIONS

Some limitations of this study include limited validation on a small number of in vivo data, and lack of clinical variability in our subjects, all of whom suffer from aneurysmal subarachnoid hemorrhage. Further work is planned using a larger study population with various types of ischemic disease or disease of the systemic circulation – this will provide a better handle on the clinical significance of our method. In the near future, we plan to use spatial-temporal Bayesian model involving MRFs.

## 6. CONCLUSION

We proposed a simple piecewise parametric model of the residual function, whose parameters are estimated from a spatial-temporal Bayesian formulation. The resulting optimization problem is solved via a non-linear least square solver. From the fitted residual function, reliable CTP parameter maps are obtained from low radiation dose CT data. Both quantitative and qualitative evaluation results for CBF, CBV and MTT maps are presented. The optimized MTT map has a decrease in MSE of 39% and an increase in SNR of 78.50% at low radiation dose estimated at 43 mA. An analysis of specific regions of interest indicates significantly improved quality in both the grey and white matter. These results indicate clinically significant improvement over conventional deconvolution and SVD based approach.

## REFERENCES

- [1] M. Wintermark, M. Lev, “FDA investigates the safety of brain perfusion CT,” *American Journal of Neuroradiology*, vol. 31, no. 1, p. 2 (2010).
- [2] M. Hirata, Y. Sugawara, Y. Fukutomi, K. Oomoto, K. Murase, H. Miki, and T. Mochizuki, “Measurement of radiation dose in cerebral CT perfusion study.” *Radiation medicine*, vol. 23, no. 2, p. 97 (2005).
- [3] Y. Imanishi, A. Fukui, H. Niimi, D. Itoh, K. Nozaki, S. Nakaji, K. Ishizuka, H. Tabata, Y. Furuya, M. Uzura et al., “Radiation-induced temporary hair loss as a radiation damage only occurring in patients who had the combination of MDCT and DSA,” *European radiology*, vol. 15, no. 1, pp. 41–46 (2005).
- [4] R. Latchaw, H. Yonas, G. Hunter, W. Yuh, T. Ueda, A. Sorensen, J. Sunshine, J. Biller, L. Wechsler, R. Higashida et al., “Guidelines and recommendations for perfusion imaging in cerebral ischemia: a scientific statement for healthcare professionals by the writing group on perfusion imaging, from the Council on Cardiovascular Radiology of the American Heart Association,” *Stroke*, vol. 34, no. 4, p. 1084 (2003).
- [5] M. Wintermark, “Cerebral perfusion CT: technique and clinical applications,” *Multislice CT*, pp. 111–121 (2009).
- [6] M. Sasaki, K. Kudo, and H. Oikawa, “CT perfusion for acute stroke: Current concepts on technical aspects and clinical applications,” in *International Congress Series*, vol. 1290. Elsevier, pp. 30–36 (2006).
- [7] M. Koenig, M. Kraus, C. Theek, E. Klotz, W. Gehlen, and L. Heuser, “Quantitative assessment of the ischemic brain by means of perfusionrelated parameters derived from perfusion CT,” *Stroke*, vol. 32, no. 2, p. 431 (2001).
- [8] M. Lev, A. Segal, J. Farkas, S. Hossain, C. Putman, G. Hunter, R. Budzik, G. Harris, F. Buonanno, M. Ezzeddine et al., “Utility of Perfusion-Weighted CT Imaging in Acute Middle Cerebral Artery Stroke Treated With Intra-Arterial Thrombolysis: Prediction of Final Infarct Volume and Clinical Outcome Editorial Comment: Prediction of Final Infarct Volume and Clinical Outcome,” *Stroke*, vol. 32, no. 9, p. 2021 (2001).
- [9] J. Eastwood, M. Lev, M. Wintermark, C. Fitzek, D. Barboriak, D. Delong, T. Lee, T. Azhari, M. Herzau, V. Chilukuri et al., “Correlation of early dynamic CT perfusion imaging with whole-brain MR diffusion and perfusion imaging in acute hemispheric stroke,” *American Journal of Neuroradiology*, vol. 24, no. 9, p. 1869 (2003).

- [10] P. Meier and K. Zierler, "On the theory of the indicator-dilution method for measurement of blood flow and volume," *Journal of applied physiology*, vol. 6, no. 12, p. 731 (1954).
- [11] N. Mullani and K. Gould, "First-pass measurements of regional blood flow with external detectors," *Journal of Nuclear Medicine*, vol. 24, no. 7, p. 577 (1983).
- [12] G. Gobbel and J. Fike, "A deconvolution method for evaluating indicator-dilution curves," *Physics in Medicine and Biology*, vol. 39, p. 1833 (1994).
- [13] L. Østergaard, R. Weisskoff, D. Chesler, C. Gyldensted, and B. Rosen, "High resolution measurement of cerebral blood flow using intravascular tracer bolus passages. Part I: Mathematical approach and statistical analysis," *Magnetic resonance in medicine*, vol. 36, no. 5, pp. 715–725 (1996).
- [14] K. Rempp, G. Brix, F. Wenz, C. Becker, F. Gückel, and W. Lorenz, "Quantification of regional cerebral blood flow and volume with dynamic susceptibility contrast-enhanced MR imaging." *Radiology*, vol. 193, no. 3, p. 637 (1994).
- [15] C. Lawson and R. Hanson, "Solving least squares problems". Society for Industrial Mathematics (1995).
- [16] L. Østergaard, A. Sorensen, K. Kwong, R. Weisskoff, C. Gyldensted, and B. Rosen, "High resolution measurement of cerebral blood flow using intravascular tracer bolus passages. Part II: Experimental comparison and preliminary results," *Magnetic Resonance in Medicine*, vol. 36, no. 5, pp. 726–736 (1996).
- [17] O. Wu, L. Østergaard, R. Weisskoff, T. Benner, B. Rosen, and A. Sorensen, "Tracer arrival timing-insensitive technique for estimating flow in MR perfusion-weighted imaging using singular value decomposition with a block-circulant deconvolution matrix," *Magnetic Resonance in Medicine*, vol. 50, no. 1, pp. 164–174 (2003).
- [18] E. Simoncelli and E. Adelson, "Noise removal via Bayesian wavelet coring," in *Image Processing, 1996. Proceedings., International Conference on*, vol. 1. IEEE, pp. 379–382 (1996).
- [19] M. Jansen, "Noise reduction by wavelet thresholding". Springer USA, vol. 161 (2001).
- [20] Moore, E. H. "On the reciprocal of the general algebraic matrix". *Bulletin of the American Mathematical Society* 26: 394–395 (1920).
- [21] Dempster, A.P. Laird, N.M. Rubin, D.B. "Maximum Likelihood from Incomplete Data via the EM Algorithm". *Journal of the Royal Statistical Society. Series B (Methodological)* vol. 39, no.1, pp.1–38 (1977).
- [22] G. Stewart, "Researches on the Circulation Time in Organs and on the Influences which affect it: Parts I," *The Journal of Physiology*, vol. 15, no. 1-2, p. 1 (1893).
- [23] R. Meuli, "Quantitative assessment of regional cerebral blood flows by perfusion CT studies at low injection rates: a critical review of the underlying theoretical models," *Eur. Radiol*, vol. 11, pp. 1220–1230 (2001).
- [24] A. Britten, M. Crotty, H. Kiremidjian, A. Grundy, and E. Adam, "The addition of computer simulated noise to investigate radiation dose and image quality in images with spatial correlation of statistical noise: an example application to X-ray CT of the brain," *British Journal of Radiology*, vol. 77, no. 916, p. 323 (2004).
- [25] J. Weickert, "Anisotropic diffusion in image processing". Teubner Stuttgart, vol. 1 (1998).
- [26] M. Black, G. Sapiro, D. Marimont, and D. Heeger, "Robust anisotropic diffusion," *IEEE Transactions on Image Processing*, vol. 7, no. 3, pp. 421–432 (2002).